

**Long-Lived Triplet Excited State in a Platinum(II) Perylene Monoimide Complex**

Journal:	<i>Dalton Transactions</i>
Manuscript ID	DT-ART-06-2018-002496.R1
Article Type:	Paper
Date Submitted by the Author:	15-Sep-2018
Complete List of Authors:	Yarnell, James; North Carolina State University, Department of Chemistry Chakraborty, Arnab ; North Carolina State University, Department of Chemistry Myahkostupov, Mykhaylo; North Carolina State University, Department of Chemistry Wright, Katherine; North Carolina State University, Department of Chemistry Castellano, Felix; North Carolina State University, Department of Chemistry



Journal Name

ARTICLE

Long-Lived Triplet Excited State in a Platinum(II) Perylene Monoimide Complex

James E. Yarnell^a, Arnab Chakraborty^a, Mykhaylo Myahkostupov^a, Katherine M. Wright^a, and Felix N. Castellano^{a*}

Received 00th January 20xx,
Accepted 00th January 20xx

DOI: 10.1039/x0xx00000x

www.rsc.org/

We report the synthesis and solution based photophysical properties of a new Pt(II)-terpyridine complex coupled to a perylene monoimide (PMI) chromophoric unit through an acetylene linkage. This structural arrangement resulted in quantitative quenching of highly fluorescent PMI chromophore by introducing metal character into the lowest energy singlet state, thereby leading to a formation of a long-lived PMI-ligand localized triplet excited state ($\tau = 8.4 \mu\text{s}$). Even though the phosphorescence from this triplet state was not observed, highly efficient quenching of this excited state by dissolved oxygen and the observation of singlet oxygen photoluminescence in the near-IR at 1270 nm initially pointed towards triplet excited state character. Additionally, the coincidence of the excited state absorbance difference spectra from the sensitized PMI ligand using a triplet donor and the Pt-PMI complex provided strong evidence for this triplet state assignment, which was further supported by TD-DFT calculations.

Introduction

The search for new molecular square planar Pt(II) based chromophores continues as their unique photophysical properties render them promising for incorporation into numerous applications. These include singlet oxygen photosensitization,^{1, 2} photocatalytic hydrogen production,³⁻⁹ electroluminescence,¹⁰ optical power limiting,^{4, 11-14} extrinsic luminescence probes,^{4, 15-17} among others.¹⁸⁻²⁵ Since the discovery of the first platinum diimine diacetylide complex Pt(phen)(C≡CPh)₂, by Che and co-workers in 1994, the number of complexes using a polyimine ligand with arylacetylide derivatives has markedly expanded.^{26, 27} The incorporation of a rigid terpyridine (trpy) ligand significantly decreases the rate of non-radiative decay as a result of the D_{4h} to D_{2d} distortion in the excited state when compared to the bipyridine analogues.²⁸⁻³² Unfortunately, this effect is nullified since the square planar geometry around the Pt(II) atom necessarily distorts when coordinated to the terpyridine ligand, resulting in the metal-centered (MC) excited states being lower in energy which creates an additional nonradiative pathway for excited state deactivation.²⁸⁻³² To limit the accessibility of MC excited states in these chromophores, a strong field arylacetylide subunit as

the ancillary ligand is rather effective, rendering Pt(II) terpyridyl complexes emissive at room temperature in most instances.^{33, 34}

In general, the lowest energy absorption band in Pt(II) terpyridine complexes bearing an acetylide ligand can be attributed to $d\pi(\text{Pt}) \rightarrow \pi^*(\text{trpy})$ metal-to-ligand charge transfer (MLCT) mixed with $\pi(\text{C-CR}) \rightarrow \pi^*(\text{trpy})$ ligand-to-ligand charge transfer (LLCT) transitions.³⁵⁻³⁷ These types of molecules are also known to induce strong spin-orbit coupling facilitating rapid intersystem crossing ($k_{isc} > 10^{11} \text{ s}^{-1}$) to the triplet charge transfer excited state.^{38, 39} In many instances, the $\pi \rightarrow \pi^*$ transitions originating from the terpyridine and acetylide ligands are very high in energy so the molecular photophysical properties are completely dictated by the triplet MLCT/LLCT excited states, resulting in charge transfer based photoluminescence. By introducing larger π -conjugated systems through the acetylene linkage, such as pyrene, the energy of the ligand-centered (LC) $^3(\pi \rightarrow \pi^*)$ excited-state is lowered to the point where they are either isoenergetic with or lower than the triplet charge transfer state. In these instances, the Pt(II) charge transfer states can internally sensitize the low energy ^3LC excited state localized on the acetylide moiety. Throughout the literature, numerous examples of this type of excited state behaviour have been reported utilizing stilbene,⁴⁰ naphthalene,⁴¹ anthracene,³⁴ pyrene,⁴² perylene,^{43, 44} perylenediimide,^{32, 43, 45} among others.⁴⁶⁻⁴⁸

The addition of highly absorbing organic chromophores to the acetylide moiety have the added benefit of greatly increasing the visible absorption cross-sections of the metal complex. Chromophores including perylene have been

^a Department of Chemistry, North Carolina State University, Raleigh, North Carolina, 27695-8204, United States

* E-mail: fncastel@ncsu.edu

Electronic Supplementary Information (ESI) available: [Additional static spectra, time-resolved spectra, synthetic details, and structural characterization data]. See DOI: 10.1039/x0xx00000x

recognized for their use as photostable dyes and pigments since their initial discovery in the early 1900's.⁴⁹ Since that time, their uses have expanded to many other photofunctional molecular species including optical switches,⁵⁰⁻⁵² organic light emitting diodes,⁵³⁻⁵⁵ organic field effect transistors,^{52, 56, 57} laser dyes,⁵⁸⁻⁶⁰ photovoltaic cells,^{56, 61-63} etc. due to their desirable visible light-harvesting capabilities,^{54, 64-70} variation of color through facile synthetic methods,⁷¹⁻⁷³ and high fluorescence quantum yields approaching 100%.^{74, 75} The covalent attachment of perylene derivatives to a square planar Pt(II) framework results in much higher light absorption compared to typical Pt(II) charge transfer chromophores, although the nature of the attachment and the involvement of charge transfer excited states significantly impact intersystem crossing rates. There are a few examples of perylene derivatives being σ -bonded directly to the Pt(II) metal center and, in most cases, the intersystem crossing rates in these molecules are unusually slow, resulting in a significant amount of unquenched fluorescence from the perylene chromophore with Φ_f values up to 78%.^{76, 77} The sluggish intersystem crossing rates are also observed when other organic chromophores such as anthracene, are cyclometalated to platinum(II) metal centers.⁷⁸ In other cases, where the perylene derivative is attached to the Pt(II) through an acetylide connector, the intersystem crossing rates become much faster, with little to no residual fluorescence from the perylene chromophore being observed.^{32, 43-45} The position of the heavy atom attachment to the perylene chromophore can also affect intersystem crossing rates, as documented by Dreeskamp and coworkers.⁷⁹

In this manuscript, we report the synthesis and photophysical properties of a new Pt(II)-terpyridine complex attached to a PMI chromophore through an acetylene linkage, (9-ethynyl-*N*-(2,5-di-*tert*-butylphenyl)-perylene-3,4-dicarboxylic imide)(4,4',4''-tri-*tert*-butyl-2,2':6',2''-terpyridine)platinum(II) hexafluorophosphate (**2**) (Figure 1). The photophysical behavior of **2** was fully characterized using a combination of steady-state and time-resolved spectroscopy, and compared against a free ligand, PMI-CCH (**1**) (Figure 1). The strong fluorescence from the PMI chromophore was quantitatively quenched by introducing metal character into its lowest energy singlet state, resulting in a long-lived LC (PMI-localized) triplet state. Although phosphorescence from this triplet state was not observed, highly efficient quenching of this excited state by oxygen and observation of singlet oxygen emission near ~ 1270 nm pointed to its triplet character. The coincidence of the excited state absorbance difference spectra from the sensitized PMI ligand (**1**) using a triplet donor and the Pt-PMI complex (**2**) provided strong evidence for this triplet state assignment, which was further supported by TD-DFT calculations.

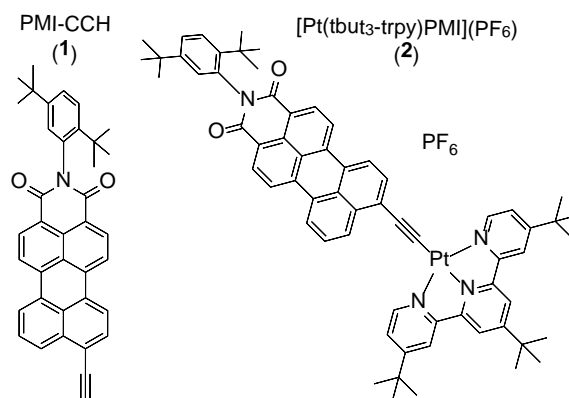


Figure 1. Structures of target chromophores used in this study: PMI-CCH (**1**) and Pt-PMI (**2**).

Experimental

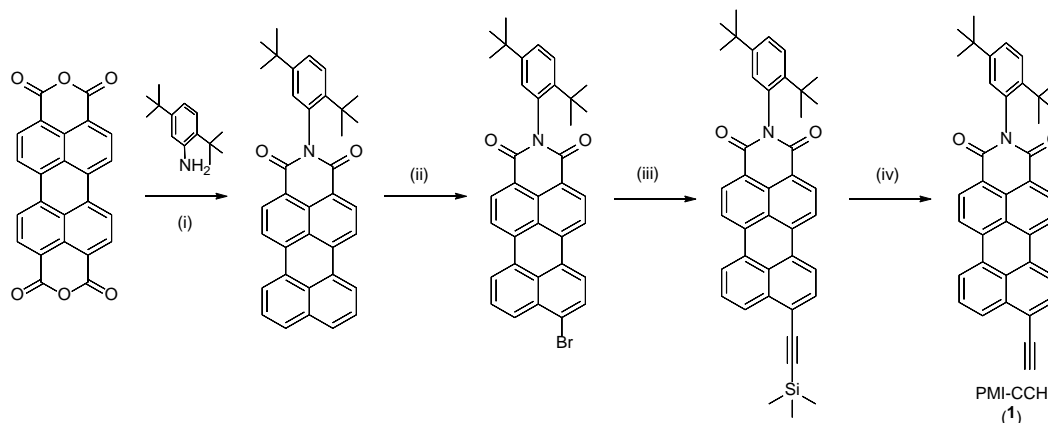
Reagents and Chemicals. All synthetic manipulations were performed under inert nitrogen atmosphere using standard Schlenk techniques. All reagents were purchased from Sigma-Aldrich or Alfa Aesar and were used as received. Spectroscopic samples were prepared using spectrophotometric grade solvents and were deaerated using the freeze-pump-thaw technique.

N-(2,5-di-*tert*-butylphenyl)-perylene-3,4-dicarboxylic imide, PMI.

Perylene monoimide (PMI) was synthesized using modified literature procedure (Scheme 1).⁸⁰ The product was isolated in 16% yield. ¹H NMR (400 MHz, CDCl₃) δ 8.63 (d, *J* = 8.0 Hz, 2H), 8.42 (t, *J* = 7.3 Hz, 4H), 7.90 (d, *J* = 8.1 Hz, 2H), 7.67 – 7.57 (m, 3H), 7.46 (dd, *J* = 8.6, 2.3 Hz, 1H), 7.04 (d, *J* = 2.3 Hz, 1H), 1.34 (s, 3H), 1.30 (s, 3H).

9-bromo-*N*-(2,5-di-*tert*-butylphenyl)-perylene-3,4-dicarboxylic imide, PMI-Br.

PMI-Br was synthesized using modified literature procedure (Scheme 1).⁸¹ *N*-bromosuccinimide (534 mg, 3.0 mmol) was added to a stirring solution of PMI (1.36 g, 2.67 mmol) in anhydrous DMF (90 mL) at room temperature under nitrogen. The reaction mixture was heated to 40 °C for 48 hours. After cooling to room temperature, the reaction mixture was poured into water (500 mL). The precipitated product was collected by filtration, washed with water (2 x 50 mL) and dried under vacuum to afford 1.04 g (66%) of PMI-Br as yellow solid. ¹H NMR (400 MHz, CDCl₃) δ 8.64 (t, *J* = 7.1 Hz, 2H), 8.46 (dd, *J* = 12.9, 7.8 Hz, 2H), 8.39 (d, *J* = 8.1 Hz, 1H), 8.30 (d, *J* = 8.5 Hz, 1H), 8.22 (d, *J* = 8.2 Hz, 1H), 7.90 (d, *J* = 8.0 Hz, 1H), 7.72 (t, *J* = 8.0 Hz, 1H), 7.59 (d, *J* = 8.6 Hz, 1H), 7.46 (d, *J* = 8.6 Hz, 1H), 7.03 (d, *J* = 2.4 Hz, 1H), 1.33 (s, 9H), 1.30 (s, 9H).

Scheme 1. Synthetic route used to prepare the PMI-CCH (**1**) ligand.^a

^aReagents and Conditions: (i) Perylene-3,4,9,10-tetracarboxylic dianhydride, 2,5-di-*tert*-butyl-aniline, zinc acetate, imidazole, and water were heated to 190 °C for 22 hours. (ii) *N*-bromosuccinimide was added PMI in anhydrous DMF and heated to 40 °C for 48 hours. (iii) PMI-Br, Pd(PPh₃)₄, and CuI were added to a 1:1 mixture of anhydrous dichloromethane/diisopropylamine along with trimethylsilylacetylene and heated to 60 °C for 36 hrs under nitrogen. (iv) PMI-CCTMS was added to K₂CO₃ in a mixture of water, methanol, and CHCl₃ and stirred at RT overnight.

9-(trimethylsilylethynyl)-N-(2,5-di-*tert*-butylphenyl)-perylene-3,4-dicarboxylic imide, PMI-CCTMS. PMI-CCTMS was synthesized using commonly employed Sonogashira cross-coupling conditions (Scheme 1).⁸²⁻⁸⁴ The product was isolated in 90% yield. ¹H NMR (400 MHz, CDCl₃) δ 8.65 (dd, *J* = 8.1, 3.7 Hz, 2H), 8.52 – 8.39 (m, 4H), 8.36 (d, *J* = 8.0 Hz, 1H), 7.81 (d, *J* = 7.9 Hz, 1H), 7.72 (t, *J* = 7.9 Hz, 1H), 7.59 (d, *J* = 8.6 Hz, 1H), 7.49 – 7.43 (m, 1H), 7.03 (d, *J* = 2.4 Hz, 1H), 1.33 (s, 9H), 1.30 (s, 9H), 0.38 (s, 9H).

9-ethynyl-N-(2,5-di-*tert*-butylphenyl)-perylene-3,4-dicarboxylic imide, PMI-CCH (1**).** Following a typical deprotection procedure, PMI-CCTMS (0.198 g, 0.327 mmol) was added under ambient conditions to a vigorously stirred solution of K₂CO₃ (0.456 g, 3.3 mmol) in a mixture of water (4 mL), methanol (20 mL) and chloroform (40 mL).^{83, 84} The reaction mixture was stirred overnight at room temperature. The reaction mixture was evaporated to dryness, the obtained residue was washed with water (2 x 25 ml) and dried under vacuum. There was observed ~8 nm blue shift in the main absorption band confirming that the deprotection was complete (Figure S1). The product was isolated as deep red solid in 73% yield (0.127 mg). ¹H NMR (CDCl₃): 8.66 (d, 2H), 8.46 (m, 4H), 8.39 (d, 1H), 7.86 (d, 1H), 7.73 (t, 1H), 7.58 (d, 1H), 7.44 (d, 1H), 7.03 (s, 1H), 3.68 (s, 1H), 1.33 (s, 9H), 1.26 (s, 9H). ¹³C NMR (CD₂Cl₂) δ 165.33, 150.85, 144.79, 137.42, 136.96, 134.81, 134.20, 132.39, 132.14, 132.02, 131.46, 130.56, 130.28, 129.78, 129.36, 129.30, 128.57, 128.23, 127.99, 127.13, 126.51, 124.68, 123.31, 122.84, 122.26, 122.02, 121.45, 121.16, 85.53, 81.69, 36.01, 34.75, 32.02, 31.56. ESI-HRMS. Found: *m/z* 534.2435 (MH⁺). Calcd for C₃₈H₃₂NO₂: *m/z* 534.2433. Anal. Calcd (found) for C₃₈H₃₁NO₂·0.8CHCl₃: C, 74.07 (74.24); H, 5.09 (5.19); N, 2.23 (2.24). ATR-FTIR: 412, 479, 532, 612, 643, 700, 734, 753, 806, 1179, 1246, 1356, 1575, 1589, 1654, 1699, 2864, 2952, 3304 cm⁻¹.

Bis(dimethyl-sulfoxide)platinum(II) dichloride, Pt(DMSO)₂Cl₂. Pt(DMSO)₂Cl₂ was synthesized using a common literature procedure

(Scheme 2).⁸⁵ The product was isolated in 80% yield and used in the next step without further purification.

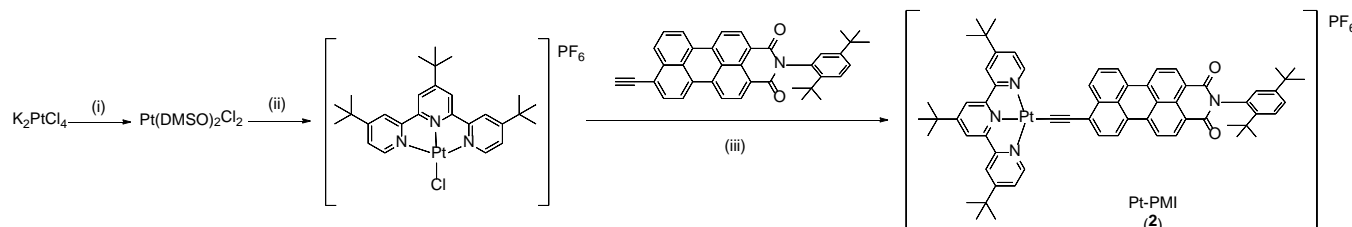
Chloro(4,4',4''-tri-*tert*-butyl-2,2':6',2''-terpyridine) platinum(II), [Pt(tbut₃-trpy)Cl](PF₆). [Pt(tbut₃-trpy)Cl](PF₆) was synthesized using a typical literature procedures (Scheme 2). The product was isolated in 93% yield and used without further purification. ¹H NMR (CD₃CN): 8.82 (d, 2H), 8.30 (s, 4H), 7.79 (d, 2H), 1.54 (s, 9H), 1.46 (s, 18H).⁸⁶

(9-ethynyl-N-(2,5-di-*tert*-butylphenyl)-perylene-3,4-dicarboxylic imide)(4,4',4''-tri-*tert*-butyl-2,2':6',2''-terpyridine)platinum(II) hexafluorophosphate, [Pt(tbut₃-trpy)PMI](PF₆) (2**).** [Pt(tbut₃-trpy)Cl](PF₆) (200 mg, 0.26 mmol), PMI-CCH (155 mg, 0.29 mmol), CuI (25 mg, 0.13 mmol), and diisopropylamine (15 mL) were added to anhydrous dichloromethane (15 mL) under nitrogen. The reaction mixture was stirred at room temperature for 24 hours (Scheme 2). Volatiles were removed under vacuum and the product was purified by alumina column chromatography eluting with acetonitrile - toluene (1:1) to afford a purple solid in 42% yield (140 mg). ¹H NMR (CD₂Cl₂): 9.29 (d, 2H), 8.67 (d, 1H), 8.43 (d, 2H), 8.27 (d, 1H), 8.16 (s, 3H), 8.09 (m, 4H), 7.76 (d, 1H), 7.67 (m, 2H), 7.53 (dd, 2H), 7.45 (dd, 1H), 7.28 (s, 1H), 1.61 (s, 9H), 1.45 (s, 18H), 1.31 (s, 9H), 1.27 (s, 9H). ¹³C NMR (CD₂Cl₂) δ 168.46, 167.60, 165.42, 165.40, 158.71, 155.75, 154.74, 150.74, 144.86, 137.24, 137.10, 135.05, 134.58, 131.54, 131.52, 131.00, 130.97, 130.29, 130.03, 129.49, 129.36, 128.65, 128.39, 127.60, 127.38, 127.05, 126.75, 126.50, 124.46, 123.99, 123.74, 122.63, 121.14, 121.08, 120.86, 120.66, 109.75, 102.68, 37.72, 36.75, 36.00, 34.80, 32.05, 31.68, 30.70, 30.47. ESI-HRMS. Found: *m/z* 1127.4709 (M-PF₆)⁺. Calcd for C₆₅H₆₅N₄O₂¹⁹⁴Pt: *m/z* 1127.4734. Anal. Calcd (found) for C₆₅H₆₅F₆N₄O₂Pt·1.75CH₂Cl₂·CH₃CN: C, 56.40 (56.65); H, 4.92 (5.20); N, 4.78 (4.52). ATR-FTIR: 557, 608, 732, 755, 832, 1244, 1287, 1352, 1562, 1589, 1613, 1654, 1695, 2103, 2866, 2958 cm⁻¹.



Journal Name

ARTICLE

Scheme 2. Synthetic route used to prepare the Pt-PMI complex (**2**).^a

^aReagents and Conditions: (i) Potassium tetrachloroplatinate(II) was dissolved in a mixture of DMSO and deionized water, and the reaction mixture was stirred for 3 hours at room temperature. (ii) Pt(DMSO)₂Cl₂ was added to a solution of 4,4',4''-tri-tert-butyl-2,2':6',2''-terpyridine in a mixture of dichloromethane/methanol (1:2), and the reaction mixture was refluxed for 24 hours. (iii) [Pt(tbut₃-trpy)Cl](PF₆), along with PMI-CCH, CuI, and diisopropylamine was added to anhydrous dichloromethane under N₂ and stirred at room temperature for 24 hours.

General Techniques. ¹H and ¹³C NMR spectra were recorded on a Varian Inova 400 NMR operating at working frequencies of 400 and 100 MHz for ¹H and ¹³C, respectively. Optical steady-state absorption spectra were measured on Cary 60 UV-vis and Shimadzu UV-3600 spectrophotometers. Steady-state photoluminescence spectra were recorded on Edinburgh FS 920 fluorescence spectrometer. Quantum yield measurements were performed on deaerated samples using rhodamine 6G in ethanol as a standard (λ_{em} 510 nm, $\Phi = 0.94$).⁸⁷ Singlet oxygen quantum yield measurements were conducted in toluene and the photoluminescence (1200-1350 nm) was collected using the Edinburgh FS 920 fluorescence spectrometer equipped with the Hamamatsu NIR detector. Singlet oxygen quantum yield values were reported relative to ZnTPP ($\Phi_{\Delta} = 0.93$ in air).⁸⁸ High-resolution electrospray mass spectrometry was carried out by the Michigan State University Mass Spectrometry Core, East Lansing, MI. Elemental analysis data was measured by Atlantic Microlab, Inc., Norcross, GA.

Ultrafast Transient Absorption Spectroscopy. Time-resolved transient absorption measurements were performed at the NCSU Imaging and Kinetic Spectroscopy (IMAKS) Laboratory in the Department of Chemistry described previously.⁸⁹ Briefly, the 800 nm laser pulses were produced at a 1 kHz repetition rate by a mode-locked Ti:sapphire laser (Coherent Libra). The pulse width was determined to be (fwhm) 105 fs using an autocorrelator. The output from the Libra was split into pump and probe beams. The pump beam was directed into a parametric amplifier (Coherent OPerA Solo) to generate the 525/550 nm excitation. The probe beam was delayed in a 6 ns optical delay stage and then focused into a sapphire crystal for white light continuum generation between 425 and 800 nm. The pump beam was focused into an 800 μ m spot on the sample and overlapped with the probe beam (~ 200 μ m). The relative

polarizations of the pump and probe beams were set at the magic angle of 54.7°. Samples under investigation were contained in 2 mm path length quartz cuvettes, and each solution was stirred continuously throughout the course of the experiment. The ground state absorption spectra were taken before and after each experiment to ensure there was no sample degradation. The transient kinetic data was evaluated using the fitting routines available in OriginPro 2016.

Nanosecond Transient Absorption Spectroscopy. Nanosecond transient absorption measurements were carried out on a LP920 laser flash photolysis system (Edinburgh Instruments) described previously.⁹⁰ Samples were prepared to have optical densities between 0.3 and 0.5 at the excitation wavelength (530 nm, 3.0 mJ/pulse) and deaerated using the freeze-pump-thaw technique in 1 cm path length quartz optical cells. All flash photolysis experiments were performed at room temperature. The reported difference spectra and kinetic data are the average of 50 laser shots. The ground state absorption spectra were taken before and after each experiment to ensure there was no sample degradation. The transient kinetic data were evaluated using the fitting routines available in OriginPro 2016.

Time-Correlated Single Photon Counting (TCSPC). Time-resolved fluorescence experiments were conducted using a time-correlated single photon counting (TCSPC) spectrometer (Edinburgh Instruments, LifeSpec II). Fluorescence signals were measured using a microchannel plate photomultiplier tube (Hamamatsu R3809U-50) in a Peltier-cooled housing. A Ti:Sapphire laser (Chameleon Ultra II, Coherent) was utilized as the excitation light source. For fluorescence intensity decay measurements, the Chameleon laser was tuned to 1080 nm, pulse picked to a 4 MHz repetition rate (Coherent 9200 Pulse Picker), and frequency doubled (APE-GmbH SHG Unit) to afford sample excitation, $\lambda_{ex} = 540$ nm.

Density Functional Theory Calculations. Calculations on **1** and **2** were performed using the Gaussian 09 software package (revision D.01)⁹¹ and the computation resources of the North Carolina State University High Performance Computing Center. Geometry optimizations were performed on the ground state and the lowest energy triplet state using the B3LYP,^{92, 93} CAM-B3LYP,⁹⁴ M06,⁹⁵ and PBE0 functionals,⁹⁶ with the SSD ECP for the Pt core electrons,⁹⁷ the Def2-SVP basis set on all atoms.⁹⁸ The polarizable continuum model (PCM) was used to simulate the effects of the dichloromethane solvent environment for all calculations.⁹⁹ The GD3 dispersion correction was applied to all optimized structures.¹⁰⁰ Frequency calculations were performed on all ground state and triplet state structures and no imaginary frequencies were obtained for any of the optimized geometries. Time dependent DFT calculations were performed on the optimized ground-state geometries using the CAM-B3LYP, B3LYP, M06, and PBE0 functionals mentioned previously. The energy and oscillator strength were computed for each of the 50 lowest singlet excitations and 10 lowest triplet excitations.

Results and Discussion

Electronic Structure Calculations. Density functional theory (DFT) and TD-DFT calculations were performed on **1** and **2** to provide insight into the nature of the photoexcited states present in these molecules. The ground state structures were optimized using the M06, PBE0, and B3LYP hybrid functionals, as well as the range corrected CAM-B3LYP functional, using Grimme's D3 dispersion correction. The optimized ground state structures of the PMI model were very similar across all four functionals, showing consistent results. The optimized ground state structure of **2** was also shown to vary minimally with selected functionals, although some small changes in the dihedral angle between the Pt-terpy and PMI were observed. The plane consisting of the Pt-terpy was found to vary between 35.7-40.9° with respect to the PMI chromophore, depending on functional used for the DFT calculation (Supporting Information, Figure S18). Because of the acetylene spacer between the two moieties, the rotational energies are likely very small, therefore at room temperature in solvent, the dihedral angle likely varies a great deal, resulting in a range on conjugation across the two parts of the molecule. The bonding environment around the platinum was also compared across functionals (Supporting Information, Figure S18). The distorted square planar environment around the Pt(II) in **2** was shown to be consistent regardless of hybrid functional used. The optimized triplet excited-state structure (and environment around the Pt(II) centre) showed little change as well, signifying that little metal charge transfer was involved in the optimized triplet state.

The molecule orbital diagrams for the frontier orbitals of **1** and **2** are presented in Figure 2. In both **1** and **2**, the HOMO-1 resides mostly on the phenyl ring attached to the imide and the HOMO resides mainly of the PMI chromophore. In **2**, there is a small portion of platinum contribution to the HOMO. In **1**, the LUMO, LUMO+1, and LUMO+2 all reside on the PMI as π^* contributions. Complex **2** displays similar PMI π^* character in the

LUMO and LUMO+1 but these molecular orbitals also have significant contribution from the terpyridine aromatic system, with the LUMO+2 consisting of solely terpyridine π^* character.

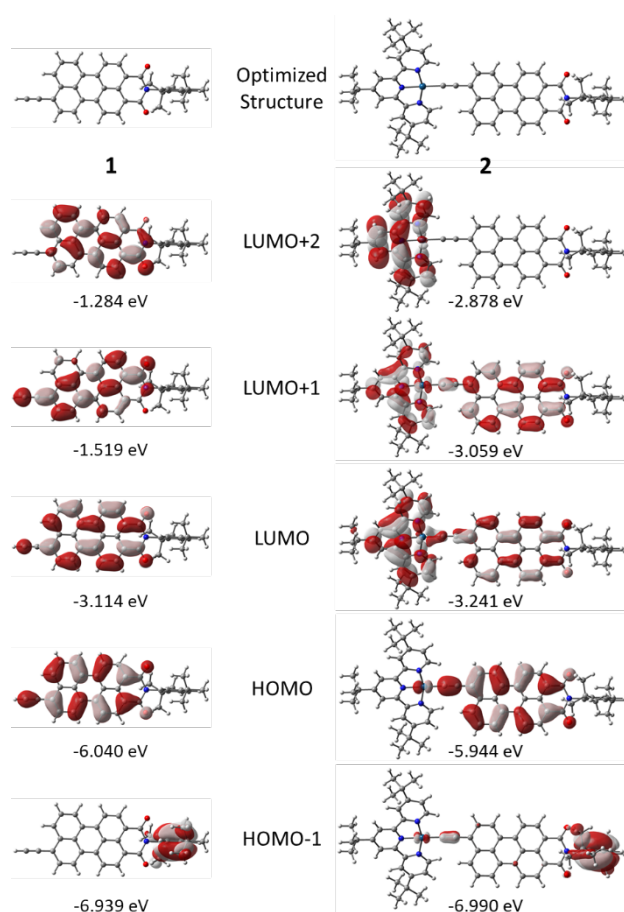


Figure 2. Frontier orbital diagram constructed for **1** and **2**. Calculations performed at M06-D3/Def2-SVP/SDD level of theory.

Absorption and Photoluminescence Spectroscopy. The electronic spectra of **1** and **2** overlaid with the calculated vertical transitions are presented in Figure 3. The low energy transitions of **1** observed in 450-550 nm range can be attributed to the π - π^* transitions of the PMI chromophore as demonstrated by the natural transition orbital analysis located in the SI. By introducing the Pt-terpy moiety to the PMI-acetylide as in **2**, the intense π - π^* transition localized on the PMI red-shifts to the 475-575 nm range, likely as a result of charge transfer character being mixed with the π - π^* transition localized on the PMI, in addition to strong σ donation accompanied by strong π back bonding from the Pt(II) metal center.^{32, 39, 43, 45, 101} This low energy band also experiences an increase in absorptivity when compared to the model. Similar to the previously reported Pt(II)-acetylide complexes, the increase in the intensity of this transition can be explained by the presence of additional charge transfer transitions which are hidden under the intense π - π^* transitions localized on the PMI, forming low energy inter-ligand charge transfer (ILCT) transitions.^{32, 44} Since there was no significant solvatochromic effect observed in the absorption

spectra of **2** (Figure S10), it is likely that the oscillator strength is due to the PMI ligand-localized transitions. The higher energy transitions observed around 325 nm are attributed to the π - π^* transitions localized on the terpyridine ligand as previously reported.^{33, 46, 102}

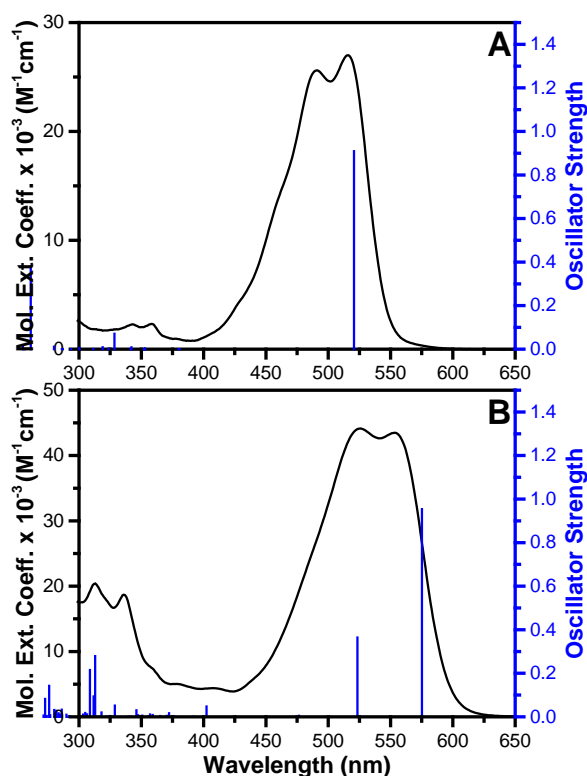


Figure 3. Electronic spectra of **1** (A) and **2** (B) in dichloromethane at room temperature. Vertical transitions (blue lines) are calculated at the TD-DFT//M06-D3/Def2-SVP/SDD level, based on optimized ground state geometries.

The TD-DFT (M06/Def2-SVP/SDD) calculations help support some of the assignments given to the electronic transitions observed in **1** and **2** with select information on the low-lying singlet excited states presented in Table 1. In both molecules, there is a good agreement with the position and intensity of the low-lying $S_0 \rightarrow S_n$ transitions observed experimentally and those calculated by TD-DFT. In **1**, the $S_0 \rightarrow S_1$ transition has a large oscillator strength ($f = 0.91$) and can be approximated as a one-electron HOMO \rightarrow LUMO transition. The $S_0 \rightarrow S_2$ and $S_0 \rightarrow S_3$ transitions are both significantly higher in energy (~ 1 eV) and have weak oscillator strength, thus not contributing much to the overall electronic spectra. In **2**, the $S_0 \rightarrow S_1$ and $S_0 \rightarrow S_2$ transitions are very similar in how the excited state density is localized since these transitions can be approximated as one-electron HOMO \rightarrow LUMO and HOMO \rightarrow LUMO+1, respectively, and LUMO and LUMO+1 are similar in appearance (Figure 2). The oscillator strength of these two transitions taken together ($f = 1.31$) results in nearly a 50% increase of absorptivity compared to **1**, thus correlating well with the experimental data. The $S_0 \rightarrow S_3$ transition can be best approximated with HOMO \rightarrow LUMO+2, but it has little oscillator strength and therefore does not

contribute significantly to the overall electronic spectra. By analysing the transition density matrix, the natural transition orbitals (NTOs) can be created to visualize the nature of the transitions (Figure 4).¹⁰³ The low-lying transitions of **2** confirm the ILCT transition assignments shown above, with $S_0 \rightarrow S_1$ and $S_0 \rightarrow S_2$ consisting of π - π^* transition localized on the PMI with substantial charge transfer to the terpyridine. The $S_0 \rightarrow S_3$ transition consists only of PMI to trpy ILCT character.

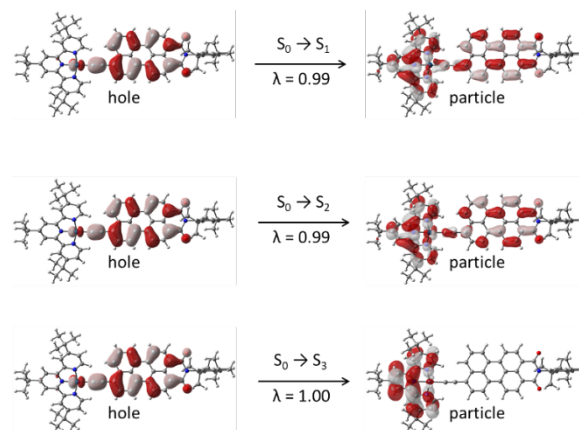


Figure 4. Natural transition orbitals (NTOs) for select $S_0 \rightarrow S_n$ excitations of **2** determined at the TD-DFT//M06-D3/Def2-SVP/SDD level of theory. λ is the fraction of the hole-particle contribution to the excitation.

Table 1. Selected electronic excitation energies (eV), corresponding oscillator strengths (f), and main configurations of the low-lying excited states of chromophores in this study.

Molecule	Electronic Transitions ^[a]	Energy ^[b] (eV)	f ^[c]	Composition	Cl ^[d]
1	$S_0 \rightarrow S_1$	2.381	0.9092	H \rightarrow L	0.7058
	$S_0 \rightarrow S_2$	3.264	0.0000	H-1 \rightarrow L	0.7012
	$S_0 \rightarrow S_3$	H-6 \rightarrow L	3.514	0.0041	0.1328
		H-4 \rightarrow L	0.5417		
		H-3 \rightarrow L	0.3303		
H-2 \rightarrow L	0.1121				
H \rightarrow L+3	0.2249				
2	$S_0 \rightarrow S_1$	2.156	0.9450	H \rightarrow L	0.6904
	H \rightarrow L+1	0.1014			
	$S_0 \rightarrow S_2$	2.369	0.3641	H \rightarrow L+1	0.6947
	$S_0 \rightarrow S_3$	H-2 \rightarrow L+2	2.602	0.0048	0.1052
H \rightarrow L+2		0.6969			

^[a] Calculated at the TD-DFT//M06-D3/Def2-SVP/SDD level, based on optimized ground state geometries. ^[b] Only the low-lying excited states were presented. ^[c] Oscillator strength. ^[d] Cl coefficients are absolute values.

The photoluminescence spectra of **1** and **2** are presented in Figure 5 with additional spectroscopic information provided in Table 2. The free ligand, **1**, had very intense photoluminescence with an emission maximum at 551 nm. The Stokes' shift, in addition to the emission quantum yield ($\Phi_{PL} = 0.85$) and the emission decay ($\tau = 4.67$ ns) are consistent with the emission originating from the S_1 excited state. When the PMI was attached to the Pt(II)-terpyridine, the photoluminescence

energy red-shifts slightly, similar to what is observed with the electronic spectra. The shoulder that appears at 550 nm was due to a minute amount of highly emissive, but difficult to remove, impurity that was still present in the sample even after several additional re-purification steps using column chromatography. In addition to the shift in energy, the emission decay time constant was reduced to <100 ps, implying that the S_1 excited state population was being quenched by an additional decay pathway not observed in **1**. Furthermore, the intensity of the prompt fluorescence was nearly quantitatively quenched ($\Phi_{PL} < 0.01$). With the covalent attachment of the Pt(II) moiety to the PMI and additional metal character in the HOMO, the intersystem crossing pathway is expected to become the predominant decay pathway from the S_1 excited state, similar to the other examples of Pt(II) acetylides attached to highly emissive chromophores.^{43, 45} When cooling the molecules to 77 K, the fluorescence peaks in both molecules blue shifted slightly (~15 nm) and the vibronic nature of each spectra sharpened. Although there was no long-lived phosphorescence observed in **2** at room temperature or 77 K, the observation of singlet O_2 (1O_2) photoluminescence centred at ~1270 nm in aerated solutions (Figure 6) indirectly supports the formation of a triplet excited state. The generation of singlet O_2 was found to be extremely efficient in aerated toluene ($\Phi_{\Delta} = 0.91$) where it was quantified relative to ZnTPP.⁸⁸ The lack of observed phosphorescence using perylene-based chromophores with low energy ligand localized triplet states has been well documented in many relevant studies,⁴³⁻⁴⁵ however, recent examples of Ru(II) and Ir(III) PDI complexes have shown that ligand-localized phosphorescence originating from a perylene chromophore is possible.¹⁰⁴⁻¹⁰⁶

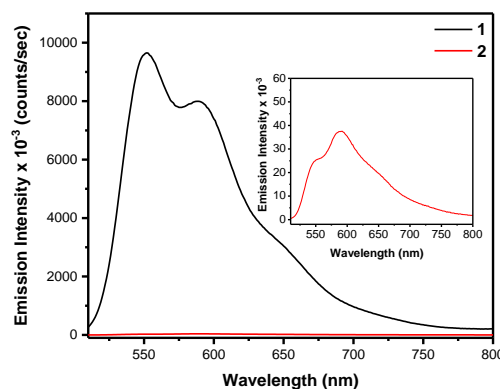


Figure 5. Photoluminescence spectra of optically matched solutions of **1** and **2** at room temperature in dichloromethane (OD = 0.1 at 500 nm). Low temperature

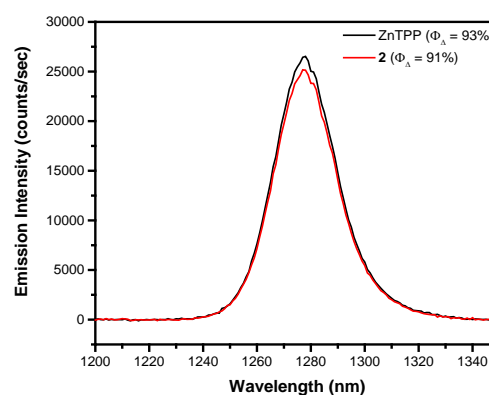


Figure 6. Near-infrared emission spectra (assigned to 1O_2 emission) of optically matched (~0.1 OD at 550 nm) ZnTPP and **2** in aerated toluene at room temperature.

Table 2. Photophysical Data of the Chromophores in This Study

molecule	$\lambda_{abs\ max}$ (nm) ($\epsilon, M^{-1}cm^{-1}$) ^[a]	Estimated oscillator strength, f	$\lambda_{em\ max}$ (nm) (298 K) ^[a]	$\lambda_{em\ max}$ (nm) (77 K) ^[b]	Φ_{Δ} (298 K) ^[c]	Φ_{em} (298 K) ^[a,d]
PMI-CCH (1)	516 (27000), 491 (25600)	0.38	551	534	0.17	0.85
Pt-PMI (2)	553 (43500), 526 (44100)	0.71	592	575	0.91	<0.01

^[a] Room temperature measurements were made using dichloromethane as the solvent. ^[b] 77 K measurements were made using 2-methyl THF as the solvent. ^[c] Singlet oxygen quantum yield measurements were performed using aerated toluene using ZnTPP in toluene as a standard ($\Phi_{\Delta} = 0.93$ in air).⁸⁸ ^[d] Quantum yield measurements were performed on deaerated samples using rhodamine 6G in ethanol as a standard (λ_{em} 510 nm, $\Phi = 0.94$).⁸⁷

Transient Absorption Spectroscopy. Ultrafast transient absorption measurements of **1** and **2** were carried out in dichloromethane solutions using 525 and 550 nm excitation, respectively. The excited state difference spectra of **1** at 500 fs has a ground state bleach at 530 nm with a shoulder at 490 nm and a broad excited state absorption at 670 nm (Figure S2). Over the course of the first 2 ps, both the ground state bleach and excited state absorbance blue-shift, likely as a result of vibrational cooling. Using the first time constant obtained from the transient decays at 550 nm and 670 nm, the observed vibrational cooling therefore occurs between 770 and 980 fs. From this point forward in time, there was no meaningful change in the difference spectra of **1**, aside from the intensity,

and a clean repopulation of the ground state was observed. In both transient decay fits, last time constant was fixed to that of the fluorescence intensity decay ($\tau = 4.67$ ns). The transient fit at 670 nm revealed a third time component ($\tau = 170$ ps) that contributes less than 9% to the overall decay. Since there are no significant changes to the observed difference spectra, this time constant likely correlates to solvent reorganization and/or small geometry changes in the molecule.

As presented in Figure 7A, the initial excited state difference spectra of **2** at 500 fs was similar to that of **1**, where the ground state bleach appears at 560 nm with a shoulder at 525 nm and the excited state absorbance has a maximum at 675 nm but now this feature extends into the NIR. Over the course of 15 ps,

a new excited state feature grows in at 620 nm while the previously described excited state feature from 650 nm to NIR decreases in intensity. Tracking the kinetics of the two bands reveal that these two features are linked as the growth at 615 nm is best fit to a biexponential ($\tau_1 = 200 \pm 30$ fs; $\tau_2 = 2.4 \pm 0.2$ ps) while the decay at 700 nm is fit to a similar biexponential ($\tau_1 = 470 \pm 45$ fs; $\tau_2 = 2.8 \pm 0.2$ ps). The ground state bleach also experiences a change in shape as the shoulder at 525 nm disappears over the same time period. The kinetic analysis at this wavelength also reveals a best fit to a biexponential function ($\tau_1 = 240 \pm 30$ fs; $\tau_2 = 3.0 \pm 0.2$ ps). The excited state features observed at 15 ps qualitatively match the excited state difference spectra obtained by Hayes and co-workers when studying a zinc-porphyrin-PMI dyad, which were assigned to the ^3PMI excited-state.¹⁰⁷ After 15 ps, the spectral features observed (Figure 7B) remain constant within the measured time window of 6 ns.

Using global fit analysis (Supporting Information, Figure S5), the excited state features observed in the fastest excited-state difference spectrum ($\tau = 171$ fs) of **2** closely match that of the singlet excited state of **1** with a broad excited state absorbance at 675 nm, which can be assigned as the depletion of the initially populated singlet excited state. Computational data shows significant d-orbital contribution to the low energy singlet transitions so this change in features is likely due to intersystem crossing. The second excited state difference spectrum ($t = 2.3$ ps) reveals changes to both the ground state bleach and excited state absorbance from the prompt features, likely due to the population of an intermediate triplet charge transfer state. The final spectrum obtained from the global fit analysis remains constant through the rest of the experiment and the transient features match to what was previously assigned to the ^3PMI excited-state. All put together, the ultrafast data reveals fast intersystem crossing ($\tau = 150$ -300 fs) from the initially populated singlet state to a high energy triplet excited state, T_n , followed by internal conversion to the long-lived, ligand localized triplet state ($\tau = 2.3$ -2.7 ps).

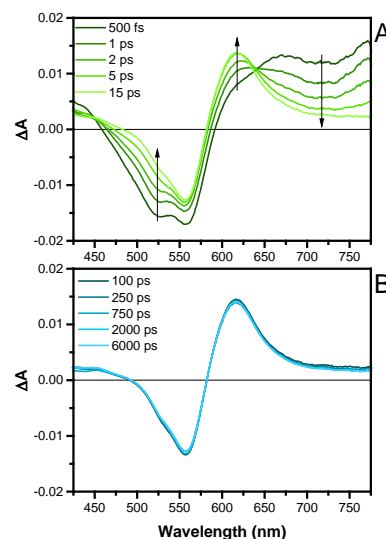


Figure 7. Excited-state absorption difference spectra of **2** in dichloromethane following 550 nm pulsed excitation (105 fs fwhm).

A nanosecond transient absorption study of **1** and **2** was carried out in deaerated dichloromethane solutions ($\lambda_{\text{ex}} = 530$ nm, 3.0 mJ/pulse, 7 ns fwhm). As presented in Figure 8, the excited state difference spectra of **2** in the nanosecond to microsecond time domains show a ground state bleach at 550 nm and an excited state absorbance at 605 nm. The features in these spectra qualitatively match the difference spectra presented in Figure 6B, signifying that the nature of the excited state observed previously has not changed between the picosecond and microsecond time domains. Both transient features observed decrease in intensity with single exponential time constants (τ at 550 nm = 8.4 μs , τ at 600 nm = 8.51 μs), indicating clean repopulation of the ground state (Figure S7). With the excited state lifetimes extending into the microseconds time regime and the excited state difference spectra matching that of the triplet sensitized ligand (discussed below), it is straightforward to assign the excited state as being ligand localized on the PMI moiety.

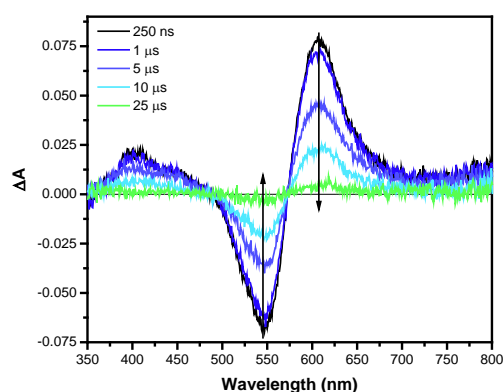


Figure 8. Excited-state absorption difference spectra of **2** in dichloromethane following 530 nm pulsed excitation (7 ns fwhm). The sample was deaerated using the freeze-pump-thaw method.

Nanosecond transient absorption spectroscopy was also performed on **1**, although in neat solution only the prompt emission and excited state difference spectra originating from the singlet excited state were observed. To study the triplet state of the PMI ligand, the sensitizer thioxanthone was used to sensitize the triplet state on the PMI through diffusional energy transfer. A solution of thioxanthone in deaerated dichloromethane was excited at 350 nm. The excited state difference spectra at 1 μ s exhibited a strong excited state absorbance at 640 nm, corresponding to the thioxanthone triplet state (Figure S8). After adding a portion of **1** to this solution, a second measurement at 10 μ s with selective excitation of the thioxanthone revealed a bleach feature at 525 nm and an excited state absorbance at 570 nm, corresponding to the PMI triplet excited state. The features of the triplet PMI difference spectra nearly quantitatively match those of the ultrafast spectra of **2** at 6 ns, as well as the nanosecond spectra, albeit shifted to lower energies, confirming the triplet assignment discussed above. Additionally, spin density calculations were performed on the optimized triplet excited state structure (M06-D3/Def2-SVP/SDD) of both **1** and **2** confirming the 3 LC assignment as much of the triplet density was localized on the PMI moiety (Figure 9). In the case of **2**, the platinum d-orbitals contribute 1.39% to the LSOMO and 0.66% to the HSOMO of the optimized triplet state.¹⁰⁸

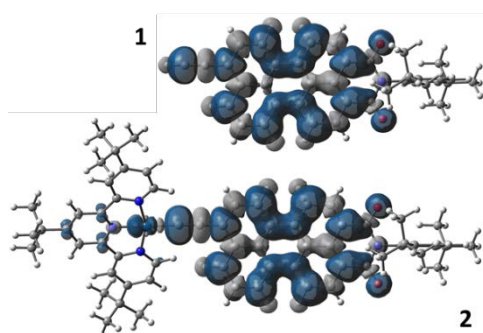


Figure 9. Isosurfaces of spin density of **1** and **2** at the lowest triplet energy (isovalue = 0.0004). Calculation was performed at M06-D3/Def2-SVP/SDD level of theory.

Figure 10 depicts the excited state decay processes observed in **2**. As illustrated by the DFT calculations, the initially populated excited state (when excited at 550 nm) is likely ligand localized on the PMI moiety with some amount of ligand-to-ligand charge transfer character from the PMI to the terpyridine. The initial difference spectrum obtained by ultrafast spectroscopy changes quickly with growth and decay features corresponding to fast intersystem crossing ($\tau = 150$ -300 fs) followed by internal conversion to the low energy ligand localized triplet state ($\tau = 2.3$ -2.7 ps). The excited state difference spectrum obtained at 15 ps persist through the duration of the ultrafast experiment and well into the microsecond time domain, returning to the ground state with a time constant of 8.4 μ s.

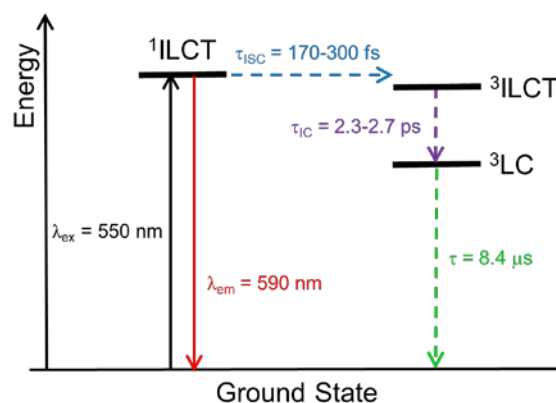


Figure 10. Energy level diagram describing the photophysical processes of **2** in DCM at room temperature. The solid lines represent radiative transitions and the dashed lines represent nonradiative transitions.

Conclusions

A comprehensive photophysical investigation has been performed on a new Pt(II)-terpyridine complex (**2**) coupled to a PMI chromophoric unit through an acetylide linkage. Phosphorescence emission was not observed directly from **2**; however, highly efficient quenching by dissolved oxygen and the observation of sensitized singlet oxygen photoluminescence in the near-IR spectral region was consistent with triplet excited state character of **2**. Ultrafast transient absorption experiments confirmed fast intersystem crossing of the initially formed ligand-localized excited state in **2**, resulting in quantitative quenching of the highly fluorescent appended PMI chromophore. The subsequent excited state absorption features were indicative of the formation of PMI ligand-localized triplet excited state which persisted with a lifetime of 8.4 μ s as measured using conventional transient absorption spectroscopy. Density functional calculations confirmed experimental determinations regarding the triplet nature of the excited states in **2**. The combined finding here suggests that the triplet excited states in perylenemonoimide chromophores can be readily accessed using Pt(II)-acetylide bonding motifs.

Acknowledgements

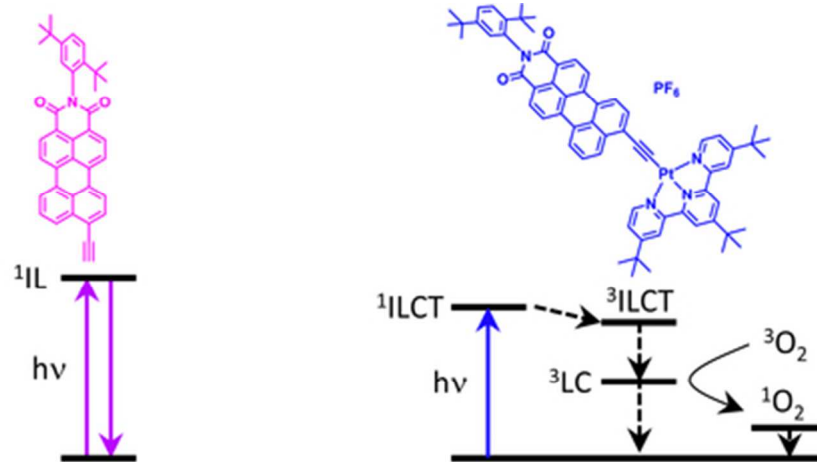
This work was supported by the U.S. Department of Energy, Office of Science, Office of Basic Energy Sciences, under Award Number DE-SC0011979. J.E.Y. was supported by the Air Force Institute of Technology (AFIT).

References

1. D. Zhang, L.-Z. Wu, Q.-Z. Yang, X.-H. Li, L.-P. Zhang and C.-H. Tung, *Org. Lett.*, 2003, **5**, 3221-3224.
2. Y. Yang, D. Zhang, L.-Z. Wu, B. Chen, L.-P. Zhang and C.-H. Tung, *J. Org. Chem.*, 2004, **69**, 4788-4791.
3. D. Zhang, L.-Z. Wu, L. Zhou, X. Han, Q.-Z. Yang, L.-P. Zhang and C.-H. Tung, *J. Am. Chem. Soc.*, 2004, **126**, 3440-3441.
4. I. Eryazici, C. N. Moorefield and G. R. Newkome, *Chem. Rev.*, 2008, **108**, 1834-1895.

5. P. Du, K. Knowles and R. Eisenberg, *J. Am. Chem. Soc.*, 2008, **130**, 12576-12577.
6. P. Du, J. Schneider, P. Jarosz and R. Eisenberg, *J. Am. Chem. Soc.*, 2006, **128**, 7726-7727.
7. P. Du, J. Schneider, P. Jarosz, J. Zhang, W. W. Brennessel and R. Eisenberg, *J. Phys. Chem. B*, 2007, **111**, 6887-6894.
8. P. Jarosz, P. Du, J. Schneider, S.-H. Lee, D. McCamant and R. Eisenberg, *Inorg. Chem.*, 2009, **48**, 9653-9663.
9. R. Narayana-Prabhu and R. H. Schmehl, *Inorg. Chem.*, 2006, **45**, 4319-4321.
10. S. C. Chan, M. C. Chan, Y. Wang, C. M. Che, K. K. Cheung and N. Zhu, *Chem. Eur. J.*, 2001, **7**, 4180-4190.
11. W. Sun, Z.-X. Wu, Q.-Z. Yang, L.-Z. Wu and C.-H. Tung, *Appl. Phys. Lett.*, 2003, **82**, 850-852.
12. F. Guo, W. Sun, Y. Liu and K. Schanze, *Inorg. Chem.*, 2005, **44**, 4055-4065.
13. F. Guo and W. Sun, *J. Phys. Chem. B*, 2006, **110**, 15029-15036.
14. Z. Ji, Y. Li and W. Sun, *Inorg. Chem.*, 2008, **47**, 7599-7607.
15. K. M.-C. Wong, W.-S. Tang, B. W.-K. Chu, N. Zhu and V. W.-W. Yam, *Organometallics*, 2004, **23**, 3459-3465.
16. C. Y.-S. Chung and V. W.-W. Yam, *J. Am. Chem. Soc.*, 2011, **133**, 18775-18784.
17. C. Y.-S. Chung, K. H.-Y. Chan and V. W.-W. Yam, *Chem. Commun.*, 2011, **47**, 2000-2002.
18. Q.-Z. Yang, L.-Z. Wu, H. Zhang, B. Chen, Z.-X. Wu, L.-P. Zhang and C.-H. Tung, *Inorg. Chem.*, 2004, **43**, 5195-5197.
19. Q. Z. Yang, Q. X. Tong, L. Z. Wu, Z. X. Wu, L. P. Zhang and C. H. Tung, *Eur. J. Inorg. Chem.*, 2004, **2004**, 1948-1954.
20. V. W.-W. Yam, R. P.-L. Tang, K. M.-C. Wong and K.-K. Cheung, *Organometallics*, 2001, **20**, 4476-4482.
21. W. Lu, M. C. Chan, N. Zhu, C. M. Che, Z. He and K. Y. Wong, *Chem. Eur. J.*, 2003, **9**, 6155-6166.
22. D.-L. Ma, T. Y.-T. Shum, F. Zhang, C.-M. Che and M. Yang, *Chem. Commun.*, 2005, 4675-4677.
23. S. Chakraborty, T. J. Wadas, H. Hester, R. Schmehl and R. Eisenberg, *Inorg. Chem.*, 2005, **44**, 6865-6878.
24. E. C. H. Kwok, M. Y. Chan, K. M. C. Wong, W. H. Lam and V. W. Yam, *Chem. Eur. J.*, 2010, **16**, 12244-12254.
25. V. Guerchais and J.-L. Fillaut, *Coord. Chem. Rev.*, 2011, **255**, 2448-2457.
26. C. W. Chan, L. K. Cheng and C. M. Che, *Coord. Chem. Rev.*, 1994, **132**, 87-97.
27. F. N. Castellano, *Dalton Trans.*, 2012, **41**, 8493-8501.
28. J. G. Williams, in *Photochemistry and Photophysics of Coordination Compounds II*, Springer, 2007, pp. 205-268.
29. M. L. Muro, A. A. Rachford, X. Wang and F. N. Castellano, in *Photophysics of Organometallics*, Springer, 2009, pp. 1-35.
30. D. R. McMillin and J. J. Moore, *Coord. Chem. Rev.*, 2002, **229**, 113-121.
31. T. K. Aldridge, E. M. Stacy and D. R. McMillin, *Inorg. Chem.*, 1994, **33**, 722-727.
32. V. Prusakova, C. E. McCusker and F. N. Castellano, *Inorg. Chem.*, 2012, **51**, 8589-8598.
33. E. Shikhova, E. O. Danilov, S. Kinayyigit, I. E. Pomestchenko, A. D. Tregubov, F. Camerel, P. Retailleau, R. Ziessel and F. N. Castellano, *Inorg. Chem.*, 2007, **46**, 3038-3048.
34. F. N. Castellano, I. E. Pomestchenko, E. Shikhova, F. Hua, M. L. Muro and N. Rajapakse, *Coord. Chem. Rev.*, 2006, **250**, 1819-1828.
35. X. Zhou, H.-X. Zhang, Q.-J. Pan, B.-H. Xia and A.-c. Tang, *J. Phys. Chem. A*, 2005, **109**, 8809-8818.
36. X. J. Liu, J. K. Feng, J. Meng, Q. J. Pan, A. M. Ren, X. Zhou and H. X. Zhang, *Eur. J. Inorg. Chem.*, 2005, **2005**, 1856-1866.
37. F. Hua, S. Kinayyigit, J. R. Cable and F. N. Castellano, *Inorg. Chem.*, 2006, **45**, 4304-4306.
38. F. Guo, Y.-G. Kim, J. R. Reynolds and K. S. Schanze, *Chem. Commun.*, 2006, 1887-1889.
39. E. O. Danilov, I. E. Pomestchenko, S. Kinayyigit, P. L. Gentili, M. Hissler, R. Ziessel and F. N. Castellano, *J. Phys. Chem. A*, 2005, **109**, 2465-2471.
40. K. Haskins-Glusac, I. Ghiviriga, K. A. Abboud and K. S. Schanze, *J. Phys. Chem. B*, 2004, **108**, 4969-4978.
41. I. E. Pomestchenko and F. N. Castellano, *J. Phys. Chem. A*, 2004, **108**, 3485-3492.
42. I. E. Pomestchenko, C. R. Luman, M. Hissler, R. Ziessel and F. N. Castellano, *Inorg. Chem.*, 2003, **42**, 1394-1396.
43. E. O. Danilov, A. A. Rachford, S. Goeb and F. N. Castellano, *J. Phys. Chem. A*, 2009, **113**, 5763-5768.
44. A. A. Rachford, S. Goeb, R. Ziessel and F. N. Castellano, *Inorg. Chem.*, 2008, **47**, 4348-4355.
45. A. A. Rachford, S. Goeb and F. N. Castellano, *J. Am. Chem. Soc.*, 2008, **130**, 2766-2767.
46. X. Wang, S. b. Goeb, Z. Ji and F. N. Castellano, *J. Phys. Chem. B*, 2010, **114**, 14440-14449.
47. C. E. Whittle, J. A. Weinstein, M. W. George and K. S. Schanze, *Inorg. Chem.*, 2001, **40**, 4053-4062.
48. H. Guo, M. L. Muro-Small, S. Ji, J. Zhao and F. N. Castellano, *Inorg. Chem.*, 2010, **49**, 6802-6804.
49. R. Scholl, C. Seer and R. Weitzenböck, *Ber. Dtsch. Chem. Ges.*, 1910, **43**, 2202-2209.
50. M. P. O'Neil, M. P. Niemczyk, W. A. Svec, D. Gosztola, G. L. Gaines and M. R. Wasielewski, *Science*, 1992, **257**, 63-65.
51. B. Yoo, T. Jung, D. Basu, A. Dodabalapur, B. A. Jones, A. Facchetti, M. R. Wasielewski and T. J. Marks, *Appl. Phys. Lett.*, 2006, **88**, 082104.
52. B. A. Jones, M. J. Ahrens, M. H. Yoon, A. Facchetti, T. J. Marks and M. R. Wasielewski, *Angew. Chem.*, 2004, **116**, 6523-6526.
53. K. Sugiyasu, N. Fujita and S. Shinkai, *Angew. Chem.*, 2004, **116**, 1249-1253.
54. A. Sautter, B. K. Kaletas, D. G. Schmid, R. Dobrawa, M. Zimine, G. Jung, I. H. M. Van Stokkum, L. De Cola, R. M. Williams and F. Wuerthner, *J. Am. Chem. Soc.*, 2005, **127**, 6719-6729.
55. C. Ego, D. Marsitzky, S. Becker, J. Zhang, A. C. Grimsdale, K. Muellen, J. D. MacKenzie, C. Silva and R. H. Friend, *J. Am. Chem. Soc.*, 2003, **125**, 437-443.
56. X. Zhan, Z. a. Tan, B. Domercq, Z. An, X. Zhang, S. Barlow, Y. Li, D. Zhu, B. Kippelen and S. R. Marder, *J. Am. Chem. Soc.*, 2007, **129**, 7246-7247.
57. Z. Liu, G. Zhang, Z. Cai, X. Chen, H. Luo, Y. Li, J. Wang and D. Zhang, *Adv. Mater.*, 2014, **26**, 6965-6977.
58. R. Gvishi, R. Reisfeld and Z. Burshtein, *Chem. Phys. Lett.*, 1993, **213**, 338-344.
59. A. Harriman, G. Izzet and R. Ziessel, *J. Am. Chem. Soc.*, 2006, **128**, 10868-10875.
60. Y. Yang, G. Lin, H. Xu, M. Wang and G. Qian, *Optics Communications*, 2008, **281**, 5218-5221.

61. L. Schmidt-Mende, A. Fechtenkotter, K. Mullen, E. Moons, R. H. Friend and J. D. MacKenzie, *Science*, 2001, **293**, 1119-1122.
62. A. Breeze, A. Salomon, D. Ginley, B. Gregg, H. Tillmann and H.-H. Hörhold, *Appl. Phys. Lett.*, 2002, **81**, 3085-3087.
63. X. Kong, H. Gong, P. Liu, W. Yao, Z. Liu, G. Wang, S. Zhang and Z. He, *New J. Chem.*, 2018, **42**, 3211-3221.
64. K.-y. Tomizaki, P. Thamyongkit, R. S. Loewe and J. S. Lindsey, *Tetrahedron*, 2003, **59**, 1191-1207.
65. J. Qu, N. G. Pschirer, D. Liu, A. Stefan, F. C. De Schryver and K. Muellen, *Chem. - Eur. J.*, 2004, **10**, 528-537.
66. F. Würthner, C.-C. You and C. R. Saha-Möller, *Chem. Soc. Rev.*, 2004, **33**, 133-146.
67. C.-C. You, C. Hippus, M. Gruene and F. Würthner, *Chem. - Eur. J.*, 2006, **12**, 7510-7519.
68. X. Li, L. E. Sinks, B. Rybtchinski and M. R. Wasielewski, *J. Am. Chem. Soc.*, 2004, **126**, 10810-10811.
69. C. Addicott, I. Oesterling, T. Yamamoto, K. Muellen and P. J. Stang, *J. Org. Chem.*, 2005, **70**, 797-801.
70. G. Hu, H. S. Kang, A. K. Mandal, A. Roy, C. Kirmaier, D. F. Bocian, D. Holten and J. S. Lindsey, *RSC Advances*, 2018, **8**, 23854-23874.
71. K. Müllen, H. Quante and N. Benfaremo, *Polymeric Materials Encyclopedia*, CRC Press, Boca Raton, FL, 1996.
72. H. Quante, Y. Geerts and K. Müllen, *Chem. Mater.*, 1997, **9**, 495-500.
73. D. Inan, R. K. Dubey, N. Westerveld, J. Bleeker, W. F. Jager and F. C. Grozema, *J. Phys. Chem. A*, 2017, **121**, 4633-4644.
74. F. Würthner, *Chem. Commun.*, 2004, 1564-1579.
75. M. R. Wasielewski, *J. Org. Chem.*, 2006, **71**, 5051-5066.
76. J. E. Yarnell, I. Davydenko, P. V. Dorovatovskii, V. N. Khrustalev, T. V. Timofeeva, F. N. Castellano, S. R. Marder, C. Risko and S. Barlow, *J. Phys. Chem. C*, 2018, **122**, 13848-13862.
77. S. Lentijo, J. A. Miguel and P. Espinet, *Inorg. Chem.*, 2010, **49**, 9169-9177.
78. J. Hu, R. Lin, J. H. Yip, K.-Y. Wong, D.-L. Ma and J. J. Vittal, *Organometallics*, 2007, **26**, 6533-6543.
79. H. Dreeskamp, E. Koch and M. Zander, *Chem. Phys. Lett.*, 1975, **31**, 251-253.
80. L. Feiler, H. Langhals and K. Polborn, *Liebigs Ann./Recl.*, 1995, **1995**, 1229-1244.
81. R. H. Mitchell, Y.-H. Lai and R. V. Williams, *J. Org. Chem.*, 1979, **44**, 4733-4735.
82. M. A. Miller, R. K. Lammi, S. Prathapan, D. Holten and J. S. Lindsey, *J. Org. Chem.*, 2000, **65**, 6634-6649.
83. M. Myahkostupov, V. Prusakova, D. G. Oblinsky, G. D. Scholes and F. N. Castellano, *J. Org. Chem.*, 2013, **78**, 8634-8644.
84. M. Myahkostupov and F. N. Castellano, *Tetrahedron*, 2015, **71**, 9519-9527.
85. V. Y. Kukushkin, A. J. L. Pombeiro, C. M. P. Ferreira, L. I. Elding and R. J. Puddephatt, *Inorg. Synth.*, 2002, **33**, 189-196.
86. S.-W. Lai, M. C. W. Chan, K.-K. Cheung and C.-M. Che, *Inorg. Chem.*, 1999, **38**, 4262-4267.
87. M. Fischer and J. Georges, *Chem. Phys. Lett.*, 1996, **260**, 115-118.
88. F. Wilkinson, W. P. Helman and A. B. Ross, *J. Phys. Chem. Ref. Data*, 1993, **22**, 113-262.
89. S. Garakyaraghi, E. O. Danilov, C. E. McCusker and F. N. Castellano, *J. Phys. Chem. A*, 2015, **119**, 3181-3193.
90. J. E. Yarnell, C. E. McCusker, A. J. Leeds, J. M. Breaux and F. N. Castellano, *Eur. J. Inorg. Chem.*, 2016, **2016**, 1808-1818.
91. M. Frisch, G. Trucks, H. Schlegel, G. Scuseria, M. Robb, J. Cheeseman, G. Scalmani, V. Barone, B. Mennucci, G. Petersson, H. Nakatsuji, M. Caricato, X. Li, H. P. Hratchian, A. F. Izmaylov, J. Bloino, G. Zheng, J. L. Sonnenberg, M. Hada, M. Ehara, K. Toyota, R. Fukuda, J. Hasegawa, M. Ishida, T. Nakajima, Y. Honda, O. Kitao, H. Nakai, T. Vreven, J. A. Montgomery, Jr., J. E. Peralta, F. Ogliaro, M. Bearpark, J. J. Heyd, E. Brothers, K. N. Kudin, V. N. Staroverov, R. Kobayashi, J. Normand, K. Raghavachari, A. Rendell, J. C. Burant, S. S. Iyengar, J. Tomasi, M. Cossi, N. Rega, J. M. Millam, M. Klene, J. E. Knox, J. B. Cross, V. Bakken, C. Adamo, J. Jaramillo, R. Gomperts, R. E. Stratmann, O. Yazyev, A. J. Austin, R. Cammi, C. Pomelli, J. W. Ochterski, R. L. Martin, K. Morokuma, V. G. Zakrzewski, G. A. Voth, P. Salvador, J. J. Dannenberg, S. Dapprich, A. D. Daniels, Ö. Farkas, J. B. Foresman, J. V. Ortiz, J. Cioslowski and D. J. Fox, *Gaussian 09, revision D.01*; Gaussian, Inc.: Wallingford, CT, 2009.
92. A. D. Becke, *J. Chem. Phys.*, 1993, **98**, 1372-1377.
93. A. D. Becke, *J. Chem. Phys.*, 1993, **98**, 5648-5652.
94. T. Yanai, D. P. Tew and N. C. Handy, *Chem. Phys. Lett.*, 2004, **393**, 51-57.
95. Y. Zhao and D. G. Truhlar, *Theor. Chem. Acc.*, 2008, **120**, 215-241.
96. C. Adamo and V. Barone, *J. Chem. Phys.*, 1999, **110**, 6158-6170.
97. D. Andrae, U. Haeussermann, M. Dolg, H. Stoll and H. Preuss, *Theor. Chim. Acta*, 1990, **77**, 123-141.
98. F. Weigend and R. Ahlrichs, *Phys. Chem. Chem. Phys.*, 2005, **7**, 3297-3305.
99. M. Cossi, G. Scalmani, N. Rega and V. Barone, *J. Chem. Phys.*, 2002, **117**, 43-54.
100. S. Grimme, J. Antony, S. Ehrlich and H. Krieg, *J. Chem. Phys.*, 2010, **132**, 154104.
101. F. Hua, S. Kinayyigit, A. A. Rachford, E. A. Shikhova, S. Goeb, J. R. Cable, C. J. Adams, K. Kirschbaum, A. A. Pinkerton and F. N. Castellano, *Inorg. Chem.*, 2007, **46**, 8771-8783.
102. H.-K. Yip, L.-K. Cheng, K.-K. Cheung and C.-M. Che, *J. Chem. Soc., Dalton Trans.*, 1993, 2933-2938.
103. R. L. Martin, *J. Chem. Phys.*, 2003, **118**, 4775-4777.
104. M. Schulze, A. Steffen and F. Würthner, *Angew. Chem. Int. Ed.*, 2015, **54**, 1570-1573.
105. C. Mari, H. Huang, R. Rubbiani, M. Schulze, F. Würthner, H. Chao and G. Gasser, *Eur. J. Inorg. Chem.*, 2017, **2017**, 1745-1752.
106. F. Heinemann, J. Karges and G. Gasser, *Acc. Chem. Res.*, 2017, **50**, 2727-2736.
107. R. T. Hayes, C. J. Walsh and M. R. Wasielewski, *J. Phys. Chem. A*, 2004, **108**, 3253-3260.
108. T. Lu and F. Chen, *J. Comput. Chem.*, 2012, **33**, 580-592.



39x19mm (300 x 300 DPI)